The Astrophysical Journal, 670: L53–L56, 2007 November 20

ON THE RELATIONSHIP BETWEEN CORONAL MAGNETIC NULL POINTS AND SOLAR ERUPTIVE EVENTS

G. Barnes
Colorado Research Associates Division, NorthWest Research Associates, Boulder, CO; graham@cora.nwra.com
Received 2007 June 29; accepted 2007 October 3; published 2007 October 16

ABSTRACT

One mechanism that has been proposed for initiating coronal mass ejections (CMEs) is the "breakout" model. For this model to account for CMEs, a coronal null point must be present prior to the eruption. The relationship between the existence of coronal null points and eruptive events is investigated using a collection of over 1800 vector magnetograms from the Imaging Vector Magnetograph at Haleakalā. Each magnetogram is subjected to magnetic charge topology analysis, including determining the presence of coronal null points. It is found that the majority of events originate in regions above which no null point is found. However, a much larger fraction of active regions for which a coronal null point was found were the source of an eruption than active regions for which no null was found. The implications of these results for the breakout model are discussed.

Subject headings: Sun: corona — Sun: coronal mass ejections (CMEs) — Sun: magnetic fields

1. INTRODUCTION

A variety of models have been proposed for initiating coronal mass ejections (CMEs), including the "breakout" model (Antiochos 1998; Antiochos et al. 1999). The hallmark of this model is reconnection at a coronal magnetic null point, where the field vanishes in the solar corona. The reconnection removes the overlying field, allowing the underlying field to erupt. For this model to account for CMEs, a coronal null point must be present prior to the eruption. The relationship between the existence of coronal null points and eruptive events has been investigated using a collection of over 1800 vector magnetograms. Each magnetogram is subjected to magnetic charge topology (MCT) analysis (Baum & Bratenahl 1980; Gorbachev & Somov 1988; Priest & Forbes 1989; Lau 1993; Démoulin et al. 1994; Parnell et al. 1994), including determining the presence of coronal null points. In MCT models, each concentration of flux at the surface of the Sun is represented by a magnetic point source, and the field due to these point sources is used as a model for the coronal magnetic field. In this context, the coronal topology becomes particularly simple because each field line must start and end on a source or a magnetic null point.

A breakout "eruption" has been considered as part of an MCT model by Maclean et al. (2005). In this case, a central source of one polarity, representing a delta spot, was surrounded by three sources of the opposite polarity, which in turn were bracketed by two sources of the original polarity, and a sequence of equilibria was constructed to represent the evolution of the delta spot. The initial configuration typically had all the flux from the central source connected to the neighboring ring of three sources, but during the evolution, a new connection to a "distant" source is created by way of a global bifurcation, i.e., breakout. For example, increasing the central source strength first results in a local separator bifurcation, which produces two coronal nulls, followed by a global spine-fan bifurcation, which produces the new connection to the distant source. Thus, it has been shown that an MCT model is capable of producing the topological properties of the breakout model.

For the observations considered here, it is found that the majority of events originate in regions above which no null point is found. However, there is an extremely strong statistical relation between the presence of at least one coronal null point and eruptive events. We first describe the data used for this analysis, then summarize the way in which the MCT model is implemented, including the algorithm for locating null points. Finally, the results are discussed in the context of the magnetic breakout model and compared to the results of a recent study by Ugarte-Urra et al. (2007), who analyzed a small number (26) of events in greater detail.

2. DATA

The vector magnetic field data used here were obtained by the Mees Solar Observatory Imaging Vector Magnetograph (IVM) at Haleakalā (Mickey et al. 1996; LaBonte et al. 1999) over the time period 2001–2004 (during a time of high solar activity and after instrument upgrades). The initial sequence of the instrument's nominal observing mode includes a "survey" of each numbered NOAA active region present on the solar disk. For the present analysis, data that suffered from obvious defects were removed, as well as those that were close to the limb (centered beyond $\mu = \cos\theta \approx 0.5$). All image-plane data were resolved of the inherent 180° ambiguity in the transverse component using the University of Hawaii approach (Canfield et al. 1993; Metcalf et al. 2006), to determine the heliographic components of the magnetic field. The MCT analysis only requires the flux distribution; thus, only magnetograms containing fewer than 64 pixels above the 3 σ noise level in the vertical magnetic field were discarded; no further selection for size, bipolar nature, complexity, or event history was imposed. Additional details can be found in Leka & Barnes (2007), and the data are available on the Web.[1]

Event characteristics were extracted from the NOAA Space Environment Center "flare event prompt reports" available through the National Geophysical Data Center,[2] which compile event data from solar observing facilities including the *Geostationary Operational Environmental Satellite* (*GOES*) soft X-ray flux monitors and the USAF Solar Observing Optical Network (SOON) Hα imagers. A region was classified as eruptive if, within 24 hr after the magnetogram was acquired, the *GOES* observations included at least a C1.0 flare (peak soft X-ray flux $\geq 10^{-6}$ W m^{-2}) that was assigned an ERU tag. This tag is determined by the presence of several eruptive centers within the

[1] See http://www.cora.nwra.com/~ivm/IVM_SurveyData.
[2] See http://www.ngdc.noaa.gov.

localized area of a flare in the SOON Hα observations (K. R. Dowdy 2007, private communication). The SOON observations include off-band measurements, which provide limited velocity information. Velocities sufficient to set the ERU flag do not always lead to a CME, as would be seen by the Large Angle and Spectrometric Coronagraph Experiment; however, it is rare for a CME to occur without the ERU flag being set. The total is 1848 magnetograms of 814 distinct active regions, from 2001 to 2004, including 283 that were classified as eruptive.

3. IMPLEMENTING THE MAGNETIC CHARGE TOPOLOGY MODEL

To implement the MCT model, each magnetogram is first partitioned into flux concentrations using the algorithm described in Barnes et al. (2005) and a source is assigned to each partition, then the null points are determined based on the source properties. Below, we describe in further detail each of these steps, then show some examples of the results.

3.1. *Magnetogram Partitioning*

Following the approach of Barnes et al. (2005), we first smooth each magnetogram by performing a potential field extrapolation to a height h. Regions of each magnetogram with a vertical field strength below 3 σ are then removed from consideration. Local maxima in $|B_z|$ are identified, and region labels are propagated downhill from each maxima, which assigns a unique label to each pixel (Schrijver et al. 1997). The saddle point between each pair of neighboring partitions is identified, and if $|B_z|$ at the saddle point is within B_s of either of the local maxima, the two partitions are merged. This has the effect of simplifying regions of the same polarity of field, particularly plage, while retaining intrusions of opposite polarity, in contrast to the smoothing, which can easily remove opposite polarity intrusions. It is particularly important in looking for coronal null points to retain opposite polarity intrusions, as such null points require at least a quadrupolar field and typically are found above a field of one polarity surrounded by field of the opposite polarity, such as the example give in Antiochos (1998).

The primary parameters controlling the behavior of the partitioning are a smoothing parameter, h, and a saddle point merging parameter, B_s. A range of smoothing and saddle point parameters has been investigated, and it was found that the presence of a coronal null point is relatively insensitive to the amount of saddle point merging but does depend sensitively on the amount of smoothing. For the results presented here, a small value of $h = 0.5$ Mm was used, along with a moderate value of $B_s = 100$ G. Once the partitions have been determined, a single point source is located at the flux-weighted center of each partition, with magnitude equal to the flux in the partition.

3.2. *Null Finding*

The null-finding algorithm begins by sorting the sources into ascending (descending) order for regions with a net negative (positive) flux. Neglecting all other sources, we determine analytically the null point associated with the first two sources. Each remaining source is reintroduced, one at a time, by slowly increasing its magnitude, starting from a factor of 10^{-6} smaller than its final value. The new null point thus introduced is located from an initial guess given by considering the new source plus a uniform field equal to the field due to all the other sources at the location of the new source. This initial guess for the null location is refined using a globally convergent multidimensional Newton-Raphson root-finding algorithm (Press et al. 1992).

Each time the source flux is increased, the locations of all the null points are recomputed using their previous locations as initial guesses for the Newton-Raphson algorithm. In addition, checks are made for local separator bifurcations (Brown & Priest 1999) and for local double-separator (or pitchfork) bifurcations (Brown & Priest 2001). A local separator bifurcation results in the creation of two new nulls of opposite types at a distance from any existing null points. When this occurs in the photosphere, one of the new nulls must be an upright null, and its appearance can be deduced by following the fan traces of the existing nulls. When a fan trace ends on a new (upright) null, the vicinity of the upright null is also searched for the second null. A local double-separator bifurcation occurs when a first-order null briefly forms a third-order null before splitting into three first-order nulls. In this process, the middle eigenvalue of the single null becomes small, so a check is made for local double-separator bifurcations whenever the middle eigenvalue is much smaller than the other two (which must be approximately equal in magnitude to satisfy $\nabla \cdot \boldsymbol{B} = 0$). The Newton-Raphson null-finding procedure is initiated at increasing distances along the eigendirection of the middle eigenvalue until a new null is found or a maximum distance is exceeded.

These procedures are likely to fail when more than one bifurcation occurs during a single incrementing of the source charge. To guard against this behavior, while also maintaining a reasonable speed for the algorithm, we check the Euler characteristics given in Longcope & Klapper (2002) once each source has been fully reintroduced. The characteristics are relations among the number of nulls of each type and sources of each polarity that must be satisfied. If they are not satisfied, at least one null point has not been located; the source is then turned off and reintroduced more slowly until the Euler characteristics are satisfied.

Satisfying the Euler characteristics does not guarantee that all null points have been found. Note, however, that missing one coronal null is guaranteed to violate the Euler characteristics because of the existence of a mirror null of the same type. Thus, one must miss a *pair* of coronal nulls of opposite types in order to have the Euler characteristics satisfied. The Euler characteristics are satisfied for all the regions considered; thus, we believe it is likely that most, if not all, of the coronal null points have been located. To confirm this, for the 92 eruptive cases in 2001, the results of this null-finding procedure have been compared to the results of one developed by C. Beveridge (2008, in preparation); the number of coronal nulls found agrees in all cases.

3.3. *Examples of the MCT Analysis*

The analysis of these data shows that coronal null points are associated with active regions with a wide range of complexity, while not all large and seemingly complex active regions result in a coronal null. Figure 1 shows examples of regions with and without coronal nulls. NOAA AR 09607 (*top left*) was found to have four coronal nulls and produced multiple eruptive events in the 24 hr following the observation. On the other hand, NOAA AR 09447 (*top right*) also has a coronal null, but did not produce any eruptive events, while NOAA AR 09727 (*bottom left*) produced an eruptive event but was not found to have a coronal null. Finally, NOAA AR 09433 (*bottom*

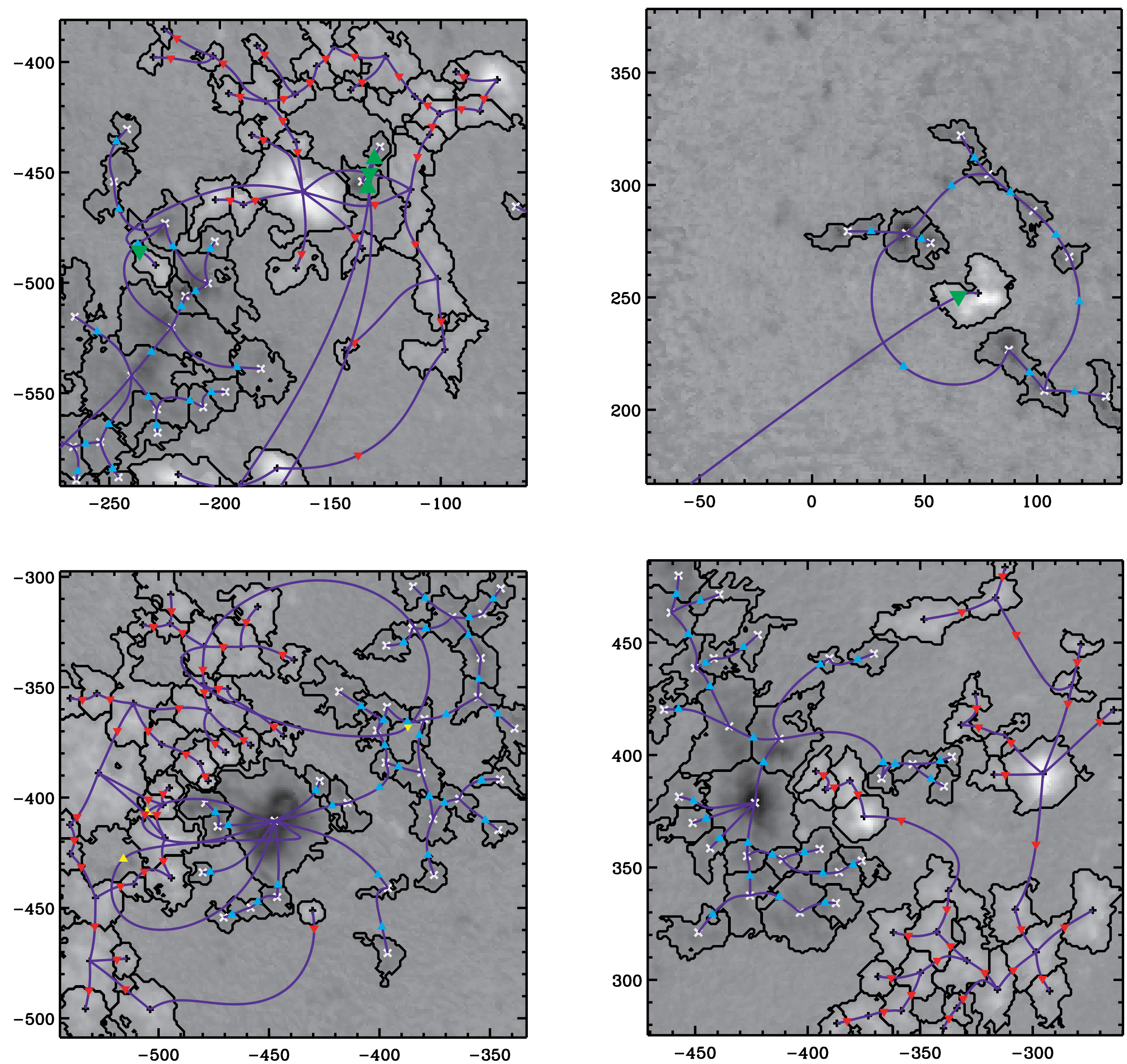

FIG. 1.—Examples of the MCT analysis of four regions, demonstrating the range in complexity of regions that give rise to coronal null points. The vertical magnetic field is shown on a gray scale; the borders of the partitions are outlined, and the sources are shown with plus signs and crosses for positive and negative sources. The magnetic null points are shown as triangles (green for coronal projected onto the photosphere, red/blue for A/B-type prone photospheric, yellow for upright photospheric), and the spine field lines are shown as purple curves. *Top left*: NOAA AR 09607 produced several eruptive events in the 24 hr following the observation; four coronal null points were found for this region. *Top right*: NOAA AR 09447 produced no eruptive events; one coronal null point was found. *Bottom left*: NOAA AR 09727 produced an eruptive event; no coronal null point was found. *Bottom right*: NOAA AR 09433 produced no eruptive event; no coronal null point was found.

right) produced neither an eruptive event nor a coronal null, despite qualitatively appearing similar to regions that did produce either an event or a null or both.

Note that in the top right panel, the spine field lines of the photospheric nulls form a closed curve that marks the intersection of the coronal null's separatrix surface with the photosphere. This closed curve is a typical signature of the presence of a single coronal null.

4. RESULTS AND DISCUSSION

Table 1 shows the frequency with which eruptive events originate from active regions with and without at least one associated coronal null point having been found. No distinction is made about the presence of multiple coronal null points, although they are present in a significant number of cases, and any null point that lies above the plane of the sources is con-

TABLE 1
OBSERVED FREQUENCIES

Active Region Type	Event	No Event
Coronal null(s)	75	141
No coronal null	209	1423

sidered a coronal null, even though some of the nulls are found at very low heights. It is evident that the majority of eruptive events (74%) occur in regions where no coronal null point was found. Thus, we conclude that it is unlikely that the breakout model can explain all eruptive events.

This is consistent with the study of Ugarte-Urra et al. (2007), who concluded that 27% of the events they considered were consistent with the breakout model and 46% were not consistent, while it was unclear in the remaining 27% whether the breakout model was responsible. However, it is interesting to note that 73% of their events came from a region where a coronal null point was found, which is much higher than the fraction in the present study. This may be a selection effect, as Ugarte-Urra et al. (2007) note that *Transition Region and Coronal Explorer* observations, which they required be available, are biased toward large flaring active regions. Unfortunately, there is almost no overlap in the events considered, so it is difficult to determine what else may contribute to the difference.

Unlike the study of Ugarte-Urra et al. (2007), regions that did not give rise to an eruptive event were also included here, so it is possible to examine the relationship between the occurrence of an event and the presence of a null. A χ^2 test of the observed frequencies indicates that the probability of these frequencies occurring if eruptive events occur independently of finding one or more coronal nulls is $<10^{-6}$; a coronal null was found for only about 9% of regions that did not produce an event, compared to 26% of the regions that did produce an event. Clearly, finding a coronal null point is much more likely for regions that give rise to an eruptive event. Alternatively, one can view the presence of a coronal null as an indication that an active region is more likely to produce an eruption, as 35% of the regions for which a null was found produced eruptions, compared with only 13% of regions for which no null was found.

Three explanations for this are possible. The simplest explanation is that the breakout model only describes some (∼26%) eruptive events and another mechanism gives rise to the remainder. A second explanation is that another mechanism gives rise to all eruptive events, but that coronal null points are more likely to be found in configurations favorable to the other mechanism. In this case, it is not the presence of the coronal null that results in the eruption, but rather the presence of the coronal null is a by-product of what gives rise to the eruption.

Finally, it is possible that the breakout model does describe most (all) eruptive events, and the analysis presented here is simply not finding all the relevant coronal null points. There are a variety of reasons that this could be the case. It may be that a coronal null point forms less than 24 hr before an event. In particular, if one typically forms about 6 hr before an event, this would be consistent with the fraction of events associated with coronal nulls in this study. This explanation is supported by the work of Gorbachev et al. (1988), who found that a small change in the photospheric field can cause a coronal null point to move a large distance along a separator, suggesting that coronal nulls may be short-lived. Instead, it may be that null points are present in the real coronal field that are not present in the MCT model field. This could happen if the real coronal field is (very) far from potential, if the use of point sources significantly changes the coronal topology, or if the limited field of view of the IVM does not include some of the flux needed to produce the coronal null. Finally, it may simply be that the null-finding algorithm is not finding all the null points. Some of the above possibilities can (and will) be explored, to further constrain whether the breakout model does explain CMEs.

Thanks to the referee for comments that improved the presentation of several aspects of the work, to K. D. Leka for developing the database, and to D. W. Longcope and C. Beveridge for discussions on null finding. This material is based on work supported by the National Science Foundation under grant 0454610 and by the Air Force Office of Scientific Research under contract F49620-03-C-0019.

REFERENCES

Antiochos, S. K. 1998, ApJ, 502, L181
Antiochos, S. K., DeVore, C. R., & Klimchuk, J. A. 1999, ApJ, 510, 485
Barnes, G., Longcope, D. W., & Leka, K. D. 2005, ApJ, 629, 561
Baum, P. J., & Bratenahl, A. 1980, Sol. Phys., 67, 245
Brown, D. S., & Priest, E. R. 1999, Proc. R. Soc. London A, 455, 3931
———. 2001, A&A, 367, 339
Canfield, R. C., et al. 1993, ApJ, 411, 362
Démoulin, P., Henoux, J. C., & Mandrini, C. H. 1994, A&A, 285, 1023
Gorbachev, V. S., Kel'ner, S. R., Somov, B. V., & Shvarts, A. S. 1988, Soviet Astron., 32, 308
Gorbachev, V. S., & Somov, B. V. 1988, Sol. Phys., 117, 77
LaBonte, B., Mickey, D. L., & Leka, K. D. 1999, Sol. Phys., 189, 1
Lau, Y.-T. 1993, Sol. Phys., 148, 301
Leka, K. D., & Barnes, G. 2007, ApJ, 656, 1173
Longcope, D. W., & Klapper, I. 2002, ApJ, 579, 468
Maclean, R., Beveridge, C., Longcope, D., Brown, D., & Priest, E. 2005, Proc. R. Soc. London A, 461, 2099
Metcalf, T. R., et al. 2006, Sol. Phys., 237, 267
Mickey, D. L., Canfield, R., LaBonte, B. J., Leka, K. D., Waterson, M. F., & Weber, H. M. 1996, Sol. Phys., 168, 229
Parnell, C. E., Priest, E. R., & Golub, L. 1994, Sol. Phys., 151, 57
Press, W. H., Teukolsky, S. A., Vetterling, W. T., & Flannery, B. P. 1992, Numerical Recipes in C: The Art of Scientific Computing (2nd ed.; New York: Cambridge Univ. Press)
Priest, E. R., & Forbes, T. G. 1989, Sol. Phys., 119, 211
Schrijver, C. J., Hagenaar, H. J., & Title, A. M. 1997, ApJ, 475, 328
Ugarte-Urra, I., Warren, H. P., & Winebarger, A. R. 2007, ApJ, 662, 1293